Available online at www.sciencedirect.com
SCIENCE DIRECT®
International Journal of Solids and Structures 43 (2006) 2989–3005
INTERNATIONAL JOURNAL OF SOLIDS and STRUCTURES
www.elsevier.com/locate/ijsolstr

Asymptotic fields around an interfacial crack with a cohesive zone ahead of the crack tip

W. Zhang, X. Deng *

Department of Mechanical Engineering, University of South Carolina, 300 Main Street, Columbia, SC 29208, USA

Received 31 January 2005; received in revised form 13 June 2005
Available online 19 August 2005

Abstract

This paper considers an interfacial crack with a cohesive zone ahead of the crack tip in a linearly elastic isotropic bi-material and derives the mixed-mode asymptotic stress and displacement fields around the crack and cohesive zone under plane deformation conditions (plane stress or plane strain). The field solution is obtained using elliptic coordinates and complex functions and can be represented in terms of a complete set of complex eigenfunction terms. The imaginary portion of the eigenvalues is characterized by a bi-material mismatch parameter $\varepsilon = \operatorname{arctanh}(\beta)/\pi$, where β is a Dundurs parameter, and the resulting fields do not contain stress singularity. The behaviors of "Mode I" type and "Mode II" type fields based on dominant eigenfunction terms are discussed in detail. For completeness, the counterpart for the Mode III solution is included in an appendix.

Keywords: Asymptotic field; Interfacial crack; Bi-material; Cohesive zone

1. Introduction

The interfacial crack problem is often encountered in investigations of geological fault lines, welded/bonded joints, layered material systems and composite materials. Much research has been conducted to understand the mechanical behavior and failure of bi-material interfaces in the presence of interfacial cracks (e.g., Williams, 1959; England, 1965; Ting, 1986, 1996; Rice, 1988; Keer and Guo, 1990; Suo and Hutchinson, 1990; Aravas and Sharma, 1991; Deng, 1993, 1995).

Using an eigenfunction expansion approach, Williams (1959) first discovered the oscillatory behavior of the in-plane linear elastic stress field near the tip of an interfacial crack. England (1965) noted that

* Corresponding author. Tel.: +1 803 777 7144; fax: +1 803 777 0106.
E-mail address: deng@engr.sc.edu (X. Deng).

0020-7683/$ - see front matter © 2005 Elsevier Ltd. All rights reserved.
doi:10.1016/j.ijsolstr.2005.06.064

the oscillatory singularity of the interfacial fields leads to crack surface overlapping and wrinkling, which are viewed as physically inadmissible although they are confined in a very small region close to the crack tip (England, 1965; Erdogan, 1965). Attempts have been made to mathematically remove the oscillation by considering contact between crack surfaces (Comninou, 1977) or transition of material properties at the interface (Atkinson, 1977). Both of these models work well in terms of removing stress oscillation and surface overlapping (Comninou, 1990), but the stress singularity remains at the crack tip. Aravas and Sharma (1991) considered frictionless contact of an interface crack between an elastoplastic material and a rigid substrate and showed that the contact zone is small under predominantly tensile loading conditions.

More recently, cohesive zone models have been found useful in dealing with fracture of joints or interfaces between dissimilar materials (e.g., Mohammed and Liechti, 2000; Madhusudhana and Narasimhan, 2002; Blackman et al., 2003; Feraren and Jensen, 2004; Tvergaard, 2004). The cohesive zone models usually employ a prescribed cohesive law (traction–separation relation) that serves as the constitutive equation of the interface. The stress singularity is eliminated by the cohesive zone models and the issue of crack surface overlapping may be resolved if the crack closure behavior (contact between crack/cohesive surfaces) is also modeled.

In this work, the interfacial crack problem is analyzed with consideration of a cohesive zone ahead of the crack tip, which serves to remove stress singularity. For the purpose of asymptotic analysis, a semi-infinite interfacial crack is taken to lie between two bonded half spaces made of dissimilar, linearly elastic, isotropic and homogeneous materials, and the deformation is assumed to be planar (plane stress or plane strain). The complex variable method and elliptic coordinates are exploited to obtain asymptotic stress and displacement fields around the interfacial crack tip and the cohesive zone.

The current study is an extension of recent investigations by the current authors (Zhang and Deng, 2005a,b) in which a cohesive zone was assumed to exist ahead of the crack tip in a homogeneous material and the eigenfunction expansion method was used to obtain the elastic fields in the near-tip region. It was found that by introducing a cohesive zone ahead of a crack, admissible non-singular crack-tip field solutions can be derived, which may assist in the formulation of possible cohesive zone models. The present study applies the same method to the bi-material interface crack problem and derives the mixed-mode asymptotic stress and displacement fields around the crack and cohesive zone under plane deformation conditions (plane stress or plane strain).

The relevance of the current work can be viewed in several ways. First, it seems that the effect of the existence of a cohesive zone ahead of an interface crack on the near-tip stress and displacement fields has not been studied analytically in the literature. The field solutions obtained in this study can serve as a basis for further studies in this area and for understanding and modeling the behavior of bi-material interfaces. Second, the proposed approach provides a way of addressing the stress oscillation issue in the interface crack problem. The method is still within the framework of linear elasticity and the solution can be obtained using the complex variable method. More complicated models that consider full-field plasticity and contact zone (e.g., Aravas and Sharma, 1991) typically require finite element analysis tools to obtain solutions.

In Section 2, mixed-mode field solutions satisfying equilibrium and compatibility conditions are derived for a homogeneous material. In Section 3, the mixed-mode fields are applied to a bi-material and the boundary conditions along the bonded interface and the traction-free crack surfaces are enforced, and then complete complex eigenvalues are obtained for the resulting eigenvalue problem. Asymptotic stress and displacement fields based on the dominant eigenvalue are derived in Section 4 and are discussed in detail in Section 5. The main findings of this study are summarized in Section 6 with concluding remarks. The Appendix C contains the solution for the anti-plane shear case.

2. Mixed-mode field solutions for a homogeneous material

Consider a semi-infinite straight crack aligned along the interface of two bonded half spaces containing Material 1 in the upper region and Material 2 in the lower region with a line fracture process zone in the form of a cohesive zone inserted directly ahead of the crack tip (see Fig. 1).

To set up the needed elements for the bi-material case, this section considers the general mixed-mode stress and displacement field solutions that satisfy equilibrium and compatibility equations for a homogeneous material.

For convenience of mathematical treatment, especially for the ease of handling the cohesive surface boundaries, elliptic coordinates (Timoshenko and Goodier, 1951) are adopted, in which the conventional rectangular Cartesian coordinates, x and y, are related to the elliptic coordinates, u and v, through the following relationship

$$\begin{cases} x = c\cosh(u)\cos(v) \\ y = c\sinh(u)\sin(v) \end{cases} \quad (u \geqslant 0,\ -\pi \leqslant v \leqslant \pi), \tag{1}$$

where c is a parameter and is chosen to be one half of the cohesive zone size.

Fig. 2 shows a plot of the elliptic coordinates with solid lines ($u =$ constant) and dashed lines ($v =$ constant), where two coincident lines, namely $v = \pi$ and $v = -\pi$, are used to represent, respectively, the upper and lower crack surfaces. The origin of the Cartesian coordinates is located at the midpoint of the cohesive zone and corresponds to $u = 0$ and $v = \pm\pi/2$ in the elliptic coordinates. The crack tip is located at $x = -c$ and $y = 0$ ($u = 0, v = \pm\pi$). The two straight line segments with length $2c$ ($-c \leqslant x \leqslant c$, $y = 0^{\pm}$ or $u = 0$, $-\pi \leqslant v \leqslant \pi$) are used to define the upper and lower cohesive surfaces. The perfectly bonded interface is denoted by the straight line $v = 0$ ($x \geqslant c$ and $y = 0$). The upper region and the lower region correspond to $0 < v \leqslant \pi$ and $-\pi \leqslant v < 0$, respectively.

To seek general mixed-mode solutions of $u_x(x,y)$ and $u_y(x,y)$ for the displacement and $\sigma_{xx}(x,y)$, $\sigma_{xy}(x,y)$ and $\sigma_{yy}(x,y)$ for the stress under plane deformation conditions (i.e., plane stress and plane strain), the complex variable method for plane elasticity problems (Timoshenko and Goodier, 1951) is employed. For convenience, Modes I and II solutions will be derived separately, which will be combined to form the mixed-mode solutions for a homogeneous material.

In the Cartesian coordinate system, the complex variable is defined as

$$\zeta = x + \mathrm{i}y, \tag{2}$$

where i is the imaginary number $\sqrt{-1}$.

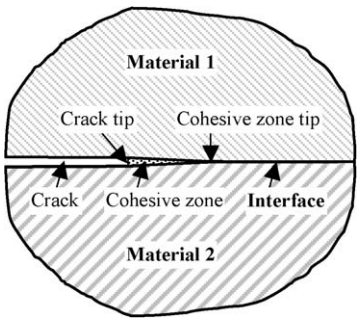

Fig. 1. A cracked bi-material plate with a cohesive zone ahead of the interface crack tip.

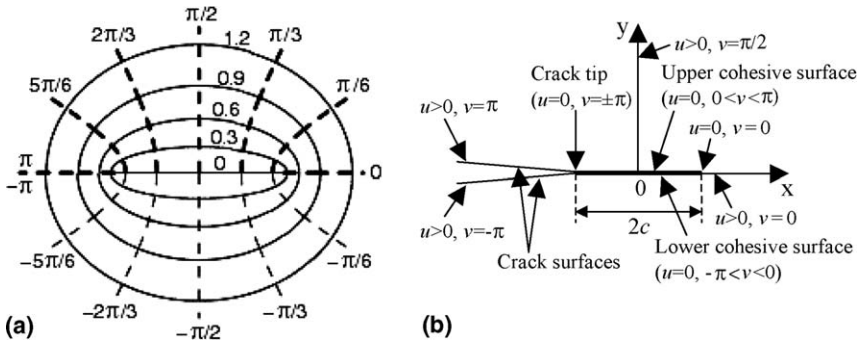

Fig. 2. A geometric description of the plane space with a crack and a cohesive zone: (a) the elliptic coordinate system with coordinates u (solid lines) and v (dashed lines); (b) locations of the crack, the crack tip and the cohesive zone in terms of elliptic coordinates. The bonded interface is represented by line $v = 0$ ($u > 0$).

According to the Kolosov–Muskhelishvili formulation, the general field solutions satisfying both the equilibrium and compatibility equations can be represented in terms of two analytic functions, $\Phi_j(\zeta)$ and $\Psi_j(\zeta)$, as follows:

$$\sigma^j_{xx} + \sigma^j_{yy} = 2[\Phi'_j(\zeta) + \bar{\Phi}'_j(\bar{\zeta})], \tag{3}$$

$$\sigma^j_{yy} + \mathrm{i}\sigma^j_{xy} = \Phi'_j(\zeta) + \bar{\Phi}'_j(\bar{\zeta}) + \bar{\zeta}\Phi''_j(\zeta) + \Psi'_j(\zeta), \tag{4}$$

$$2\mu_j(u^j_x + \mathrm{i}u^j_y) = \kappa_j\Phi_j(\zeta) - \zeta\bar{\Phi}'_j(\bar{\zeta}) - \bar{\Psi}_j(\bar{\zeta}), \tag{5}$$

where $\kappa_j = 3 - 4\nu_j$ for plane strain and $\kappa_j = (3 - \nu_j)/(1 + \nu_j)$ for plane stress, ν_j is Poisson's ratio and μ_j shear modulus of the bulk material surrounding the crack, the superscript/subscript j ($j = 1, 2$) refers to material numbers (necessary for extension to the bi-material case, to be discussed in the next section). A prime after a function implies differentiation and an over-bar denotes a complex conjugate. No summation is implied over j in Eq. (5).

Another complex variable is defined in the elliptic coordinate system as

$$\omega = u + \mathrm{i}v. \tag{6}$$

Using Eqs. (1), (2) and (6), the following conformal mapping can be established

$$\zeta = c\cosh(\omega). \tag{7}$$

It is thus noted that an analytic function of the complex variable ζ can also be written as an analytic function of the complex variable ω. The task now is to identify an analytic function that will meet the boundary conditions for a mixed-mode crack problem.

For pure Mode I or Mode II deformation, it is known that $\Phi_j(\zeta)$ and $\Psi_j(\zeta)$ can be replaced by the Westergaard function (Unger, 1995). In this study, the following form of Westergaard functions

$$Z^j_k(\zeta) = \Upsilon^j_k(\omega) = -2(\lambda + 1)(\lambda - 3)\mu_j(b_k - \mathrm{i}a_k)\left[(\lambda - 2)\mathrm{e}^{\lambda\omega} - \lambda\mathrm{e}^{(\lambda-2)\omega}\right] \tag{8}$$

are chosen, where a_k, b_k and λ are real-valued parameters. The deformation mode, namely, Modes I and II, is indicated by subscript k with $k = 1, 2$, respectively. The superscript or subscript j ($j = 1, 2$), again, refers to the material number. To be concise, the superscript j in a_k and b_k has been omitted. One should bear in mind that a_k and b_k are different in different materials.

Based on the formulations in Zhang and Deng (2005b), the mixed-mode analytic functions $\Phi_j(\zeta)$ and $\Psi_j(\zeta)$ as well as their derivatives can be obtained by combining the functions for Modes I and II (Appendix

A), and expressions of the stress and displacement fields in terms of elliptic coordinates can be derived from Eqs. (3)–(5). For instance,

$$\begin{aligned}\sigma_{yy}^{j}(u,v) &= 4\mu_j(\lambda+1)(\lambda-3)\{\lambda(a_1\sin((\lambda-2)v)+b_1\cos((\lambda-2)v))\mathrm{e}^{(\lambda-2)u}\\ &\quad+\lambda(\lambda-2)[(a_1+b_2)(\sin(\lambda v)-\sin((\lambda-2)v))+(b_1-a_2)(\cos(\lambda v)\\ &\quad-\cos((\lambda-2)v))]\sinh(u)\mathrm{e}^{(\lambda-1)u}-(\lambda-2)(a_1\sin(\lambda v)+b_1\cos(\lambda v))\mathrm{e}^{\lambda u}\},\end{aligned} \tag{9}$$

$$\begin{aligned}\sigma_{xy}^{j}(u,v) &= 4\mu_j(\lambda+1)(\lambda-3)\{\lambda(a_2\sin((\lambda-2)v)+b_2\cos((\lambda-2)v))\mathrm{e}^{(\lambda-2)\mathrm{u}}\\ &\quad+\lambda(\lambda-2)[(b_1-a_2)(\sin(\lambda v)-\sin((\lambda-2)v))-(a_1+b_2)(\cos(\lambda v)\\ &\quad-\cos((\lambda-2)v))]\sinh(u)\mathrm{e}^{(\lambda-1)u}-(\lambda-2)(a_2\sin(\lambda v)+b_2\cos(\lambda v))\mathrm{e}^{\lambda u}\}.\end{aligned} \tag{10}$$

On the upper crack surface $v=\pi$, Eq. (9) yields the normal stress

$$\sigma_{yy}^{1}(u,\pi) = -4\mu_1(\lambda+1)(\lambda-3)[(\lambda-2)\mathrm{e}^{\lambda\mathrm{u}}-\lambda\mathrm{e}^{(\lambda-2)u}](\sin(\lambda\pi)a_1+\cos(\lambda\pi)b_1). \tag{11}$$

At the bonded interface $v=0^{+}$,

$$\sigma_{yy}^{1}(u,0) = -4\mu_1(\lambda+1)(\lambda-3)[(\lambda-2)\mathrm{e}^{\lambda u}-\lambda\mathrm{e}^{(\lambda-2)u}]b_1. \tag{12}$$

For brevity, other stress components as well as the displacement components are not listed here.

3. The interface crack problem

Based on the general mixed-mode field solutions provided in the preceding section, this section enforces the boundary conditions in a bi-material and solves the resulting eigenvalue problem. Following Williams (1959), we assume that the same parameter λ in the solutions obtained in the preceding section applies to both Materials 1 and 2. To this end, it is noted that the continuity conditions at the bonded interface are independent of the coordinate u.

In terms of elliptic coordinates, the traction-free boundary conditions on the crack surfaces ($v=\pm\pi$) are

$$\sigma_{yy}^{1}(u,\pi)=\sigma_{xy}^{1}(u,\pi)=\sigma_{yy}^{2}(u,-\pi)=\sigma_{xy}^{2}(u,-\pi)=0. \tag{13}$$

The traction and displacement continuity conditions across the bonded interface ($v=0$) require that

$$\sigma_{yy}^{1}(u,0)=\sigma_{yy}^{2}(u,0),\quad \sigma_{xy}^{1}(u,0)=\sigma_{xy}^{2}(u,0), \tag{14}$$

$$u_{y}^{1}(u,0)=u_{y}^{2}(u,0),\quad u_{x}^{1}(u,0)=u_{x}^{2}(u,0). \tag{15}$$

3.1. Eigenvalues in the real space

For simplicity, we define the following parameters in terms of the shear moduli μ_1 (for Material 1) and μ_2 (for Material 2), Mode I deformation coefficients a_1, b_1 and Mode II deformation coefficients a_2 and b_2:

$$c_1=a_1\mu_1,\quad c_2=a_2\mu_1,\quad c_3=b_1\mu_1,\quad c_4=b_2\mu_1\quad\text{(for Material 1)}, \tag{16}$$

$$c_5=a_1\mu_2,\quad c_6=a_2\mu_2,\quad c_7=b_1\mu_2,\quad c_8=b_2\mu_2\quad\text{(for Material 2)}. \tag{17}$$

Note that a_k and b_k ($k=1,2$) for Material 1 have different values from those for Material 2. The traction continuity conditions (Eq. (14)) result in (e.g., see Eq. (12))

$$c_7=c_3,\quad c_8=c_4. \tag{18}$$

Making use of Eq. (18) and considering other boundary conditions shown in Eqs. (13) and (15), we have (e.g., see Eq. (11))

$$\sin(\lambda\pi)c_1 + \cos(\lambda\pi)c_3 = 0, \quad \sin(\lambda\pi)c_2 + \cos(\lambda\pi)c_4 = 0, \tag{19}$$

$$\cos(\lambda\pi)c_3 - \sin(\lambda\pi)c_5 = 0, \quad \cos(\lambda\pi)c_4 - \sin(\lambda\pi)c_6 = 0, \tag{20}$$

$$\frac{\alpha+1}{2}c_1 + \beta c_4 + \frac{\alpha-1}{2}c_5 = 0, \quad \frac{\alpha+1}{2}c_2 - \beta c_3 + \frac{\alpha-1}{2}c_6 = 0, \tag{21}$$

where α and β are Dundurs parameters (Dundurs, 1969)

$$\alpha = \frac{\mu_2(\kappa_1+1) - \mu_1(\kappa_2+1)}{\mu_2(\kappa_1+1) + \mu_1(\kappa_2+1)}, \quad \beta = \frac{\mu_2(\kappa_1-1) - \mu_1(\kappa_2-1)}{\mu_2(\kappa_1+1) + \mu_1(\kappa_2+1)}. \tag{22}$$

It has been shown that $-1 \leqslant \alpha \leqslant 1$ and $-1/2 \leqslant \beta \leqslant 1/2$ for real materials. Note that in Eqs. (19) and (20), a common factor

$$f(\lambda,u) = 4(\lambda+1)(\lambda-3)[(\lambda-2)e^{\lambda u} - \lambda e^{(\lambda-2)u}] \tag{23}$$

has been cancelled because the solutions for $f(\lambda,u)$=0, i.e., $\lambda = -1, 3$, are included in the complete eigenvalues shown later. Similarly, a common factor $g(\lambda,u)$ has been cancelled from Eq. (21), with

$$g(\lambda,u) = \frac{c}{2}e^{(\lambda-3)u}[(\lambda-2)(\lambda-3)e^{4u} - 2(\lambda+1)(\lambda-3)e^{2u} + \lambda(\lambda+1)]. \tag{24}$$

Eqs. (19)–(21) contain six unknowns c_m ($m = 1$–6) in the simultaneous, linear algebraic, homogeneous equations. Non-trivial solutions exist only if the determinant of the coefficient matrix vanishes. As such, the following characteristic equation, which defines an eigenvalue problem, must be solved:

$$\sin(\lambda\pi)^2[\cos(\lambda\pi)^2 + \beta^2\sin(\lambda\pi)^2] = 0. \tag{25}$$

Interestingly, the above equation depends on only one Dundurs parameter. It is obvious that the eigenvalues are $\lambda = n/2$ (n is an integer) for $\beta = 0$. When $\beta \neq 0$, the real eigenvalues consist of integers only (i.e. $\lambda = n$). To seek the complete eigenvalues for $\beta \neq 0$, we need to extend the solution domain to the complex space.

3.2. Eigenvalues in the complex space

Although we have assumed real values for a_1, b_1, a_2, b_2 and λ during the process of obtaining the stress and displacement components by separating the real and imaginary parts of those analytic functions in Appendix A, nothing actually prevents these constants from taking complex values once expressions for the stress and displacement components are obtained. In other words, that the stresses and displacements are real does not mean that the parameters in their expressions must be real. Essentially, we can assume

$$\lambda = \lambda_r + i\lambda_i, \tag{26}$$

where λ_r and λ_i are real-valued constants. Substituting Eq. (26) into Eq. (25) and *separating real and imaginary parts again* results in the following two equations:

$$(\beta^2-1)\cos(4\pi\lambda_r)\cosh(4\pi\lambda_i) - 4\beta^2\cos(2\pi\lambda_r)\cosh(2\pi\lambda_i) + 3\beta^2 + 1 = 0, \tag{27}$$

$$\sin(2\pi\lambda_r)\sinh(2\pi\lambda_i)[(1-\beta^2)\cos(2\pi\lambda_r)\cosh(2\pi\lambda_i) + \beta^2] = 0. \tag{28}$$

Keeping in mind that $-1/2 \leqslant \beta \leqslant 1/2$ and solving the above equations for λ_r and λ_i eventually yields the complete eigenvalues for the interface crack problem

$$\begin{cases} \lambda = \left(n - \dfrac{1}{2}\right) \pm \mathrm{i}\varepsilon, \\ \lambda = n, \end{cases} \tag{29}$$

where n is an integer and ε is a bi-material mismatch parameter given by

$$\varepsilon = \frac{\arctan h(\beta)}{\pi} = \frac{1}{2\pi} \ln\left(\frac{1+\beta}{1-\beta}\right). \tag{30}$$

Eq. (29) includes the same set of eigenvalues as in the Williams' solution that was later made complete by Lin and Mar (1976) and Symington (1987).

4. Asymptotic solution near the interface crack tip

To focus on the asymptotic behavior in the near-tip region, a solution based on a dominant eigenvalue and possessing the following features is sought: (1) stresses are finite everywhere due to the existence of the cohesive zone; (2) tractions are continuous across the cohesive surfaces; (3) there is a finite displacement jump across the cohesive surfaces; and (4) stresses tend to zero far away from the near-tip region.

A close examination of the eigenvalue terms reveals that the first feature is true for all eigenvalues in a finite domain since no singular point for u and v exists (e.g., see Eq. (9)). The second feature is also true, which can be verified by substituting $u = 0$ into Eqs. (9) and (10) for any λ and associated parameters (one example is shown below when $\lambda = -1/2 \pm \mathrm{i}\varepsilon$). Similarly, the third feature also holds true for all terms. The last feature stems from the expectation that stress concentration takes place near the crack tip, which is consistent with the classical fracture mechanics.

The eigenfunctions of the stress fields (e.g., Eq. (9)) can be regarded as terms in a Fourier series with a "frequency" spectrum. For homogeneous materials ($\varepsilon = 0$), it has been argued that the dominant eigenfunction term corresponds to the eigenvalue $\lambda = -1/2$ and other "low frequency" terms of integer eigenvalues (e.g., $\lambda = -1, 0$, etc.) can in fact be excluded from the Modes I and II crack problems (Zhang and Deng, 2005b).

For the case of a bi-material, it is also argued here that the near-tip dominant term is the one with $\lambda_r = -1/2$ when ε is small. This is because that we expect a "smooth transition" from the homogeneous case to the bi-material case, so that a very small ε should not change the dominance of the individual eigenfunctions.

For $\lambda = -1/2 + \mathrm{i}\varepsilon$, five of the six equations in Eqs. (19)–(21) can be selected to solve for the unknowns. For example, the solutions to the first five equations, in terms of c_3 that is yet to be determined, are

$$c_1 = \mathrm{i}\beta c_3, \quad c_2 = \beta c_3, \quad c_4 = -\mathrm{i}c_3, \quad c_5 = -\mathrm{i}\beta c_3, \quad c_6 = -\beta c_3. \tag{31}$$

It is noted that the above expressions remain the same for all n in $\lambda = n - 1/2 + \mathrm{i}\varepsilon$. The parameter c_3, however, changes from eigenvalue to eigenvalue. Similarly, for $\lambda = -1/2 - \mathrm{i}\varepsilon$, the constants are related by

$$c_1 = -\mathrm{i}\beta c_3, \quad c_2 = \beta c_3, \quad c_4 = ic_3, \quad c_5 = \mathrm{i}\beta c_3, \quad c_6 = -\beta c_3. \tag{32}$$

These expressions remain the same for all n in $\lambda = n - 1/2 - \mathrm{i}\varepsilon$ even though c_3 changes from eigenvalue to eigenvalue.

In practice, we can select c_3 in Eq. (32) as the conjugate of c_3 in Eq. (31) to obtain real stress and displacement fields. Hence the eigenvalue $\lambda = -1/2 + \mathrm{i}\varepsilon$ must be accompanied by $\lambda = -1/2 - \mathrm{i}\varepsilon$ at all times. Each component of stress or displacement (e.g., Eq. (9)) can be computed by adding two individual terms with conjugate eigenvalues (e.g., $\lambda = -1/2 \pm \mathrm{i}\varepsilon$) and conjugate coefficients (see Eqs. (16), (17), (31) and (32) while remembering that c_3 in Eq. (32) is selected as the conjugate of c_3 in Eq. (31)). This result is consistent with the findings by Deng (1992) who confirmed that the analytic functions must include two terms with

conjugate eigenvalues in order to obtain non-trivial solutions for the interface crack stress field of a bi-material.

Without loss of generality, let $c_3 = -p$ (a real value) and substitute it together with $\lambda = -1/2 + i\varepsilon$ into the stress and displacement fields, then repeat this procedure for $\lambda = -1/2 - i\varepsilon$ and add up the conjugate results. The resulting expressions are very lengthy and are not given here, but simpler expressions for the traction and normal displacement components along the crack line (i.e., $y = 0^{\pm}$) are given in Appendix B. A Maple 9.0 script (Maplesoft, 2004) was written to obtain the general stress and displacement field expressions.

As an example, let us consider the plane strain case ($\kappa_j = 3 - 4\nu_j$) and suppose that the materials are aluminum (Material 1) and steel (Material 2) with the following properties (Keer and Guo, 1990): $\mu_1 = 26.32$ GPa, $\nu_1 = 0.33$, $\mu_2 = 80.77$ GPa, and $\nu_2 = 0.3$. The Dundurs constant is $\beta = 0.1167$ and the bi-material mismatch parameter is $\varepsilon = 0.0373$. Contours of normalized stresses are shown in Fig. 3(a)–(c), where the rectangular coordinates are normalized by c (the half cohesive zone size) and the stress components are normalized by the quantity defined below

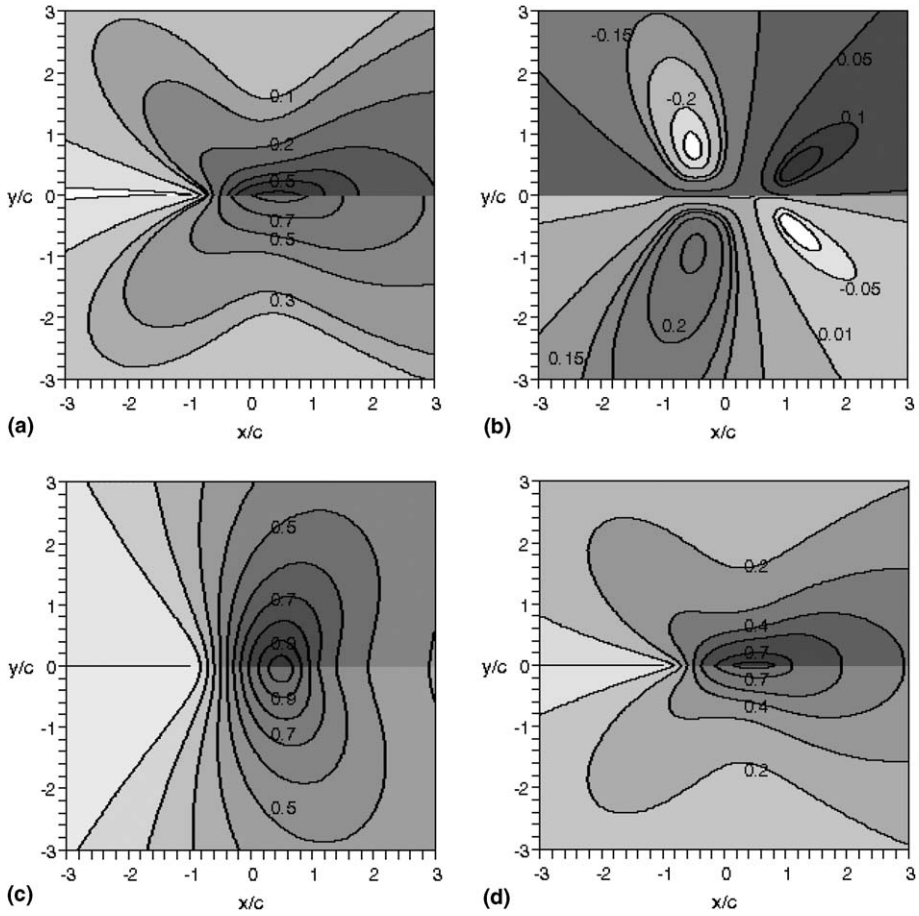

Fig. 3. Contours of normalized stresses for the case of $c_3 = -p$ ("Mode I"): (a) σ_{xx}/σ_m, (b) σ_{xy}/σ_m, (c) σ_{yy}/σ_m, and (d) σ_{xx}/σ_m for a homogeneous material (aluminum).

$$\sigma_m = \frac{3p[\sqrt{3}(12\varepsilon^2+7)\cosh(2\pi\varepsilon/3) + 8\varepsilon\sinh(2\pi\varepsilon/3)]}{\cosh(\pi\varepsilon)}. \tag{33}$$

The figures clearly show that the stress distributions in the case of a bi-material are not symmetrical with respect to the crack line $y = 0$, and that the stress component σ_{xx}/σ_m is discontinuous across the interface. For comparison, a plot of σ_{xx}/σ_m for a homogeneous material (aluminum) is shown in Fig. 3(d), where the stress distribution is seen to be continuous and symmetrical with respect to the crack line.

Fig. 4(a) shows the normalized variations of stress σ_{xx} along the upper ($y = 0^+$) and lower ($y = 0^-$) crack surfaces. Stresses σ_{xy} and σ_{yy} are continuous across $y = 0$ and their normalized variations along $y = 0$ are given in Fig. 4(b). Fig. 4(c) and (d) show the normalized variations of the displacements u_x and u_y along $y = 0$, respectively, where

$$u_m = \frac{12[\mu_2(\kappa_1+1) + \mu_1(\kappa_2+1)]cp}{\mu_1\mu_2\cosh(\pi\varepsilon)}. \tag{34}$$

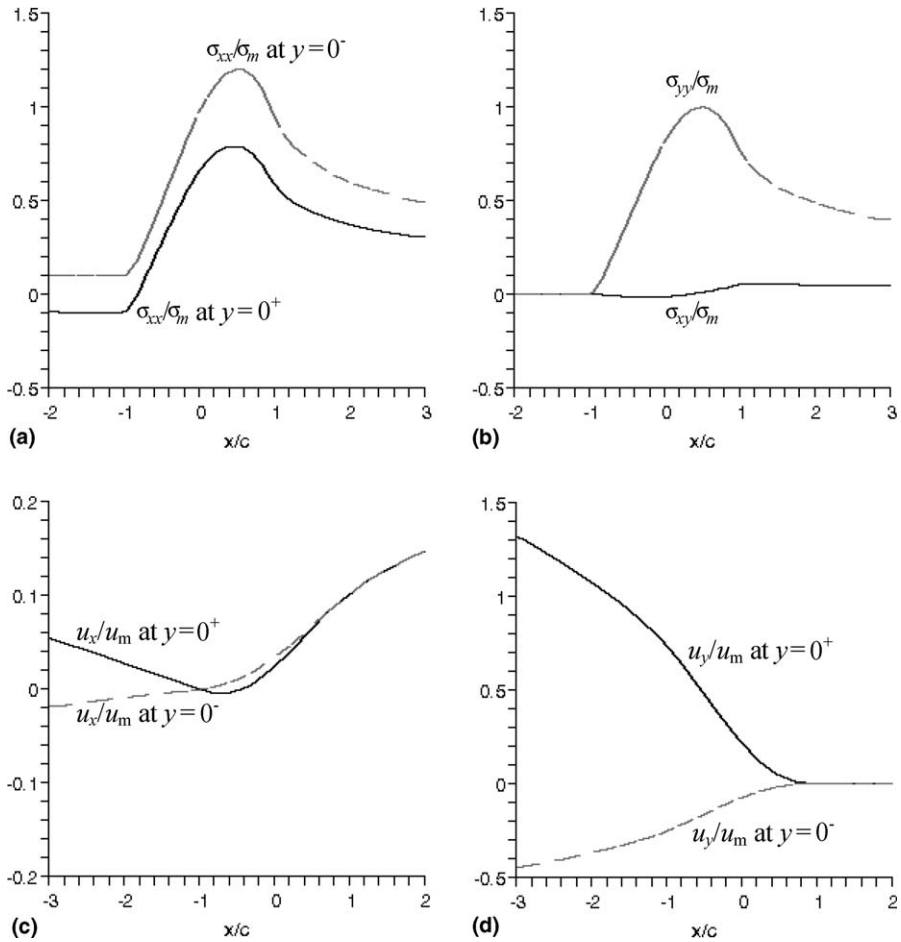

Fig. 4. Normalized variations of stresses and displacements along $y = 0$ for the case of $c_3 = -p$ (“Mode I”): (a) σ_{xx}/σ_m, (b) σ_{xy}/σ_m and σ_{yy}/σ_m, (c) u_x/u_m, and (d) u_y/u_m.

Note that we have assumed that p has the unit of GPa.

Along the cohesive zone ($u = 0$), the displacement difference between the upper and lower cohesive surfaces can be obtained from Eqs. (B.8) and (B.10) (it is noted that the displacement of the lower surface is represented by $u_y^2(0, v)$ with $-\pi \leqslant v \leqslant 0$). The displacement jump $\delta_y(v)$ across the cohesive zone is ($0 \leqslant v \leqslant \pi$)

$$\begin{aligned}\delta_y(v) &= u_y^1(0, v) - u_y^2(0, -v) \\ &= \frac{[\mu_2(\kappa_1 + 1) + \mu_1(\kappa_2 + 1)]cp}{4\mu_1\mu_2 \cosh(\pi\varepsilon)} \{24\varepsilon[\beta \cosh((\pi - v)\varepsilon) - \sinh((\pi - v)\varepsilon)][\cos(v/2) - \cos(3v/2)] \\ &\quad + [\beta \sinh((\pi - v)\varepsilon) - \cosh((\pi - v)\varepsilon)][(4\varepsilon^2 - 35)\sin(v/2) + (8\varepsilon^2 + 14)\sin(3v/2) \\ &\quad - (4\varepsilon^2 + 1)\sin(7v/2)]\}. \end{aligned} \tag{35}$$

5. Discussions

It is interesting to see from Fig. 4(a) and (b) that all stresses are finite along the interface, which is one of the desired features of the current solution. Also, Fig. 4(d) reveals that the upper crack and cohesive surfaces do not penetrate into the lower crack and cohesive surfaces. This is reasonable since σ_{yy} is tensile and its magnitude is much larger than that of the shear stress σ_{xy} (Fig. 4(b)) which changes its sign in the cohesive zone. The position of the maximum σ_{xx}/σ_m and σ_{yy}/σ_m values is very close to $x/c = 0.5$ for the bi-material case, which is slightly different from the homogeneous case in which the maximum stress occurs at exactly $x/c = 0.5$ (Zhang and Deng, 2005b). This position is inside the cohesive zone region and is closer to the cohesive zone tip (which is at $x/c = 1$) than to the crack tip (which is at $x/c = -1$).

Fig. 5 displays the normalized displacement jumps $\delta_y(v)/u_m$ for a range of ε values (with systematically varied shear moduli but constant Poisson's ratios). Here the parameter u_m is computed from Eq. (34) with $\mu_1 = 26.32$ GPa, $v_1 = 0.33$, $\mu_2 = 80.77$ GPa, and $v_2 = 0.3$. It clearly demonstrates that the cohesive surfaces will not overlap. In fact, all curves will coincide with the one for $\varepsilon = 0.0373$ if u_m varies with material

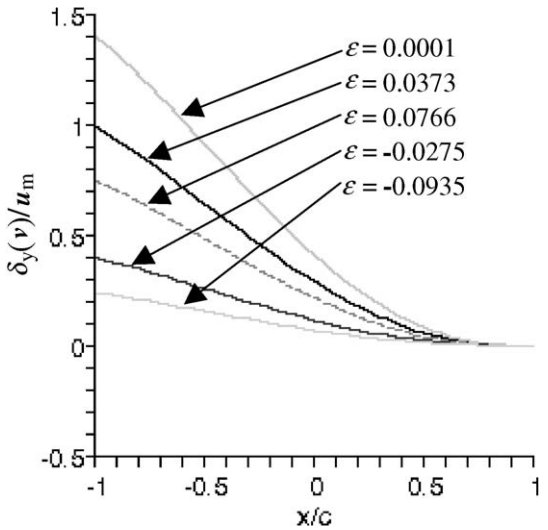

Fig. 5. Normalized variations of the displacement jump across the cohesive surfaces for a range of ε values (corresponding to systematically varied shear modulus values), where the normalizing parameter u_m is for the aluminum–steel bi-material.

properties as in Eq. (34) instead of being kept constant. Thus displacement jump behind the crack tip is always larger than zero, and hence the crack surfaces will never penetrate each other.

If the lower and upper materials are identical, say $\mu_2 = \mu_1 = 26.32$ GPa, $\nu_2 = \nu_1 = 0.33$, the Dundurs constant β and the bi-material mismatch parameter ε will both vanish. Then stresses σ_{xx} and σ_{yy} become symmetrical with respect to the crack line, and stress σ_{xy} becomes skew-symmetric and equals to zero along the interface. That is, the resulting field corresponds to a pure Mode I deformation, which has been described in Zhang and Deng (2005b). As such, the bi-material solution described in the preceding section, which is derived when c_3 is real-valued, can be loosely called the "Mode I" type.

"Mode II" solution for the bi-material case, which corresponds to a pure Mode II deformation when Materials 1 and 2 are identical, can be obtained by setting $c_3 = -ip$ (purely imaginary) for $\lambda = -1/2 \pm i\varepsilon$. For brevity, the resulting "Mode II" fields are not written out here. Using aluminum and steel material properties, the normalized variations of the stress and displacement components along $y = 0$ are plotted in Fig. 6. In this case, the upper and lower crack surfaces do overlap (Fig. 6(d)), implying potential contact. The σ_{yy} stress changes sign in the cohesive zone (Fig. 6(b)), indicating that a compressive normal

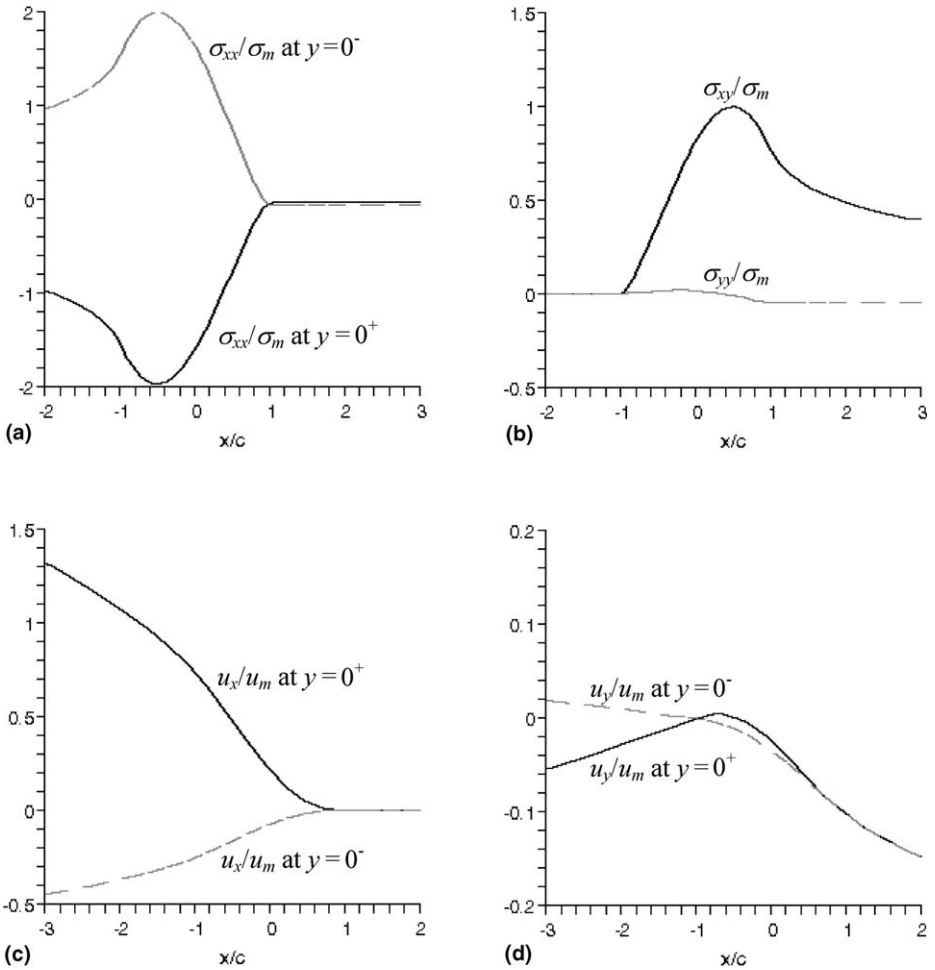

Fig. 6. Normalized variations of stresses and displacements along $y = 0$ for the case of $c_3 = -ip$ ("Mode II"): (a) σ_{xx}/σ_m, (b) σ_{xy}/σ_m and σ_{yy}/σ_m, (c) u_x/u_m, and (d) u_y/u_m. Here parameters p, σ_m and u_m have different values from those of "Mode I".

stress should develop in part of the cohesive zone. The current solution becomes invalid since the contact between crack/cohesive surfaces is not taken into account.

If the materials in the upper and lower half spaces are switched while keeping the same shear load, slightly different results will emerge from the "Mode II" solution. In particular, the variations of u_y/u_m along $y = 0$ are plotted in Fig. 7(a) when Material 1 is steel and Material 2 is aluminum. It reveals that the surface overlapping now occurs mainly in the cohesive zone. Therefore, the deformation under Mode II loading depends on the relative position of the two materials (or equivalently the shear direction without exchanging the materials). The current solution predicts that pure Mode II loading will lead to a non-overlapping displacement field only for homogeneous materials as shown in Fig. 7(b), where the upper and lower crack/cohesive surfaces always have the same displacement u_y.

So far, only solutions corresponding to real and imaginary values of c_3 have been described, which can be loosely referred to, respectively, as "Mode I" and "Mode II" solutions. The general solution for mixed-mode cases must then include both real and imaginary terms of c_3, which can be obtained by combining the "Mode I" and "Mode II" solutions. Thus, based on the dominant eigenvalue term, a mixed-mode solution for a bi-material will not lead to crack/cohesive surface contact only when there is sufficient tensile loading.

It is worth noting that solutions corresponding to "higher frequencies" (i.e., terms with eigenvalues of larger magnitude) can also be obtained by the same procedure. In general, more terms of the eigenfunctions should be used to approximate the stress fields under given boundary conditions. But, so long as the stress level resulting from other terms are much smaller than that from the dominant term, the "dominant term" solution ($\lambda = -1/2 \pm i\varepsilon$) can be used because of its simplicity.

One salient feature of the obtained solutions is that a cohesive law is not specified in advance. In general, various eigenfunction terms are expected to work together to accommodate a specific cohesive law. Alternatively, possible forms of the traction–separation relation in the cohesive zone may be extracted if particular eigenfunction terms are assumed to characterize the behavior of the cohesive zone. For example, if the dominant eigenfunction term is assumed, a "Mode I" type cohesive zone model may be formulated from the normal traction $\sigma_{yy}(v)$ (Eq. (B.2)) and the normal displacement jump $\delta_y(v)$ (Eq. (35)) along cohesive surfaces, as shown in Fig. 8, for which Material 1 is aluminum and Material 2 is steel. It is noted that the fracture energy (the area under the traction–separation curve) can be directly related to the cohesive strength (the maximum value of σ_{yy}) and the maximum separation, and these model parameters can also be related to outer-field quantities such as the stress intensity factor and J-integral during fracture (see e.g., Zhang and Deng, 2005a).

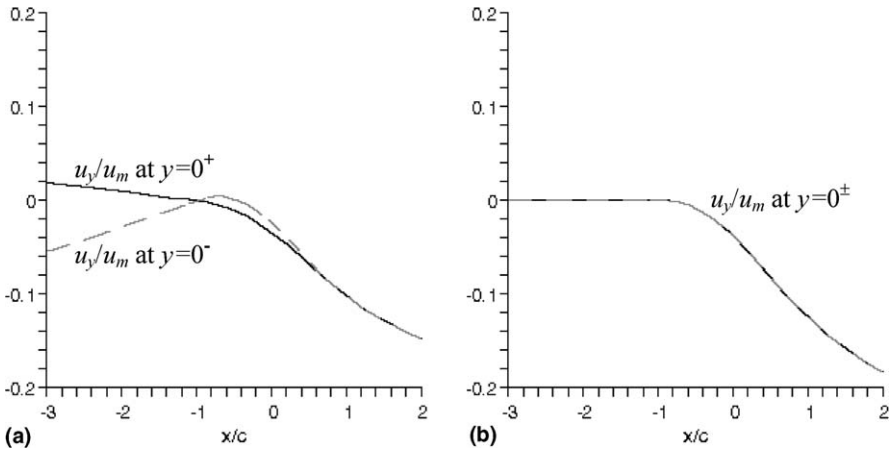

Fig. 7. Normalized variations of displacements along $y = 0$ for the case of $c_3 = -ip$ ("Mode II"): (a) u_y/u_m when upper and lower materials are exchanged; and (b) u_y/u_m in a homogeneous material (aluminum).

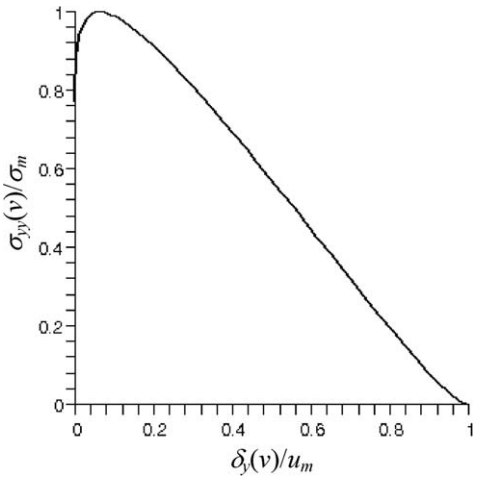

Fig. 8. A normalized "Mode I" traction–separation relation.

6. Summary and concluding remarks

With consideration of a cohesive zone ahead of the crack tip, we have obtained the near-field stresses and displacements around an interfacial crack and the cohesive zone between two dissimilar, homogeneous, and linearly elastic isotropic materials.

There are several key steps in the approach taken in this study: (1) analytic functions and elliptic coordinates are used to represent the general mixed-mode stress and displacement fields that automatically satisfy the equilibrium and compatibility conditions in a homogeneous material; (2) the mixed-mode solutions are then applied to a bi-material with the enforcement of boundary conditions along the bonded interface and the traction-free crack surfaces, which leads to an eigenvalue problem; (3) the eigenvalue problem is solved with complex eigenvalues and the unknown coefficient parameters are extended to take complex values; and (4) stress and displacement fields corresponding to each of the complex eigenfunction terms can then be derived by including their complex conjugate terms.

The general mixed-mode solution, which does not contain any stress singularity, can be considered to be a combination of a "Mode I" type solution and a "Mode II" type solution. The "Mode I" and "Mode II" solutions have been discussed by considering only the dominant eigenfunction term. It is found that, while crack surface overlapping does not occur in the "Mode I" solution, it does in the "Mode II" solution, implying crack surface contact in a "Mode II" deformation situation. To avoid crack surface contact in a mixed-mode case, a sufficiently significant "Mode I" term must be present.

The anti-plane shear (or Mode III) case is decoupled from the in-plane mixed-mode case and its solution can be obtained relatively easily. For completeness, the Mode III solution is given in Appendix C. The solution is similar to that for a homogeneous material, which has been described in an earlier investigation (Zhang and Deng, 2005a).

Acknowledgements

The authors greatly appreciate the support by the ONR DEPSCoR program (Grant # N00014-03-1-0807). They also wish to thank Dr. M.J. Rodgers for helpful discussions.

Appendix A. Analytic functions for mixed-mode crack

According to Eqs. (7) and (8), the mixed-mode functions $\Phi_j(\zeta)$ and $\Psi_j(\zeta)$ as well as their derivatives can be obtained as

$$\begin{aligned}\Phi_j''(\zeta) &= Z_1^{j'}(\zeta) - \mathrm{i}Z_2^{j'}(\zeta)\\ &= -\frac{4\lambda(\lambda+1)(\lambda-2)(\lambda-3)\mu_j(b_1-\mathrm{i}a_1)\mathrm{e}^{(\lambda-1)\omega}}{c}\\ &\quad+\frac{4\lambda(\lambda+1)(\lambda-2)(\lambda-3)\mathrm{i}\mu_j(b_2-\mathrm{i}a_2)\mathrm{e}^{(\lambda-1)\omega}}{c},\end{aligned} \tag{A.1}$$

$$\begin{aligned}\Phi_j'(\zeta) &= Z_1^{j}(\zeta) - \mathrm{i}Z_2^{j}(\zeta)\\ &= -2(\lambda+1)(\lambda-3)\mu_j(b_1-\mathrm{i}a_1)[(\lambda-2)\mathrm{e}^{\lambda\omega}-\lambda\mathrm{e}^{(\lambda-2)\omega}]\\ &\quad+2(\lambda+1)(\lambda-3)\mathrm{i}\mu_j(b_2-\mathrm{i}a_2)[(\lambda-2)\mathrm{e}^{\lambda\omega}-\lambda\mathrm{e}^{(\lambda-2)\omega}],\end{aligned} \tag{A.2}$$

$$\begin{aligned}\Psi_j'(\zeta) &= -\zeta Z_1^{j'}(\zeta)+\mathrm{i}[\zeta Z_2^{j'}(\zeta)+2Z_2^{j}(\zeta)] = 4\lambda(\lambda+1)(\lambda-2)(\lambda-3)\mu_j(b_1-\mathrm{i}a_1)\cosh(\omega)\mathrm{e}^{(\lambda-1)\omega}\\ &\quad-4\lambda(\lambda+1)(\lambda-2)(\lambda-3)\mathrm{i}\mu_j(b_2-\mathrm{i}a_2)\left[\cosh(\omega)\mathrm{e}^{(\lambda-1)\omega}+\frac{(\lambda-2)\mathrm{e}^{\lambda\omega}-\lambda\mathrm{e}^{(\lambda-2)\omega}}{\lambda(\lambda-2)}\right],\end{aligned} \tag{A.3}$$

$$\begin{aligned}\Phi_j(\zeta) &= -\mu_j(b_1-\mathrm{i}a_1)c[(\lambda-2)(\lambda-3)\mathrm{e}^{(\lambda+1)\omega}-2(\lambda+1)(\lambda-3)\mathrm{e}^{(\lambda-1)\omega}+\lambda(\lambda+1)\mathrm{e}^{(\lambda-3)\omega}]\\ &\quad+\mathrm{i}\mu_j(b_2-\mathrm{i}a_2)c[(\lambda-2)(\lambda-3)\mathrm{e}^{(\lambda+1)\omega}-2(\lambda+1)(\lambda-3)\mathrm{e}^{(\lambda-1)\omega}+\lambda(\lambda+1)\mathrm{e}^{(\lambda-3)\omega}],\end{aligned} \tag{A.4}$$

$$\begin{aligned}\Psi_j(\zeta) &= \lambda(\lambda-2)\mu_j(b_1-\mathrm{i}a_1)c[(\lambda-3)\mathrm{e}^{(\lambda+1)\omega}-(\lambda+1)\mathrm{e}^{(\lambda-3)\omega}]\\ &\quad-\mathrm{i}\mu_j(b_2-\mathrm{i}a_2)c[(\lambda+2)(\lambda-2)(\lambda-3)\mathrm{e}^{(\lambda+1)\omega}\\ &\quad-4(\lambda+1)(\lambda-3)\mathrm{e}^{(\lambda-1)\omega}-\lambda(\lambda+1)(\lambda-4)\mathrm{e}^{(\lambda-3)\omega}],\end{aligned} \tag{A.5}$$

where subscripts 1 and 2 for parameters a and b refer to the deformation mode, i.e., Modes I and II, respectively, and subscript j (j=1, 2) is the material number (note that this subscript is omitted for parameters a and b).

Appendix B. Expressions of stress and displacement fields

The general expressions for the stress and displacement fields have been obtained by using a Maple script (Maplesoft, 2004). Explicit expressions are given here only for the traction and normal displacement components along $y=0$ corresponding to $\lambda=-1/2\pm\mathrm{i}\varepsilon$.

For the case of $c_3=-p$ ("Mode I" type), the stresses and displacements along $y=0^+$ (which lies in Material 1 and covers $v=\pi$ for $x\leqslant -c$; $u=0$ and $0<v<\pi$ for $-c<x<c$; and $v=0$ for $x\geqslant c$) can be written as (note that, a superscript of 1 or 2 implies Material 1 or Material 2)

$$\sigma_{yy}^1(u,\pi)=0, \tag{B.1}$$

$$\begin{aligned}\sigma_{yy}^1(0,v) &= \frac{p}{\cosh(\pi\varepsilon)}\big[2\varepsilon(-(4\varepsilon^2-23)\sin(v/2)+(4\varepsilon^2+1)\sin(5v/2))\sinh((\pi-v)\varepsilon)\\ &\quad+((44\varepsilon^2+35)\cos(v/2)-(28\varepsilon^2+7)\cos(5v/2))\cosh((\pi-v)\varepsilon)\big],\end{aligned} \tag{B.2}$$

$$\sigma^1_{yy}(u,0) = p\mathrm{e}^{-5u/2}\left[2\varepsilon((4\varepsilon^2-23)\mathrm{e}^{2u} - 4\varepsilon^2 - 1)\sin(\varepsilon u) + ((44\varepsilon^2+35)\mathrm{e}^{2u} - 28\varepsilon^2 - 7)\cos(\varepsilon u)\right], \tag{B.3}$$

$$\sigma^1_{xy}(u,\pi) = 0, \tag{B.4}$$

$$\begin{aligned}\sigma^1_{xy}(0,v) = \frac{p}{\cosh(\pi\varepsilon)}\big[&2\varepsilon(-(4\varepsilon^2-23)\cos(v/2) + (4\varepsilon^2+1)\cos(5v/2))\cosh((\pi-v)\varepsilon)\\ &-((44\varepsilon^2+35)\sin(v/2) - (28\varepsilon^2+7)\sin(5v/2))\sinh((\pi-v)\varepsilon)\big],\end{aligned} \tag{B.5}$$

$$\sigma^1_{xy}(u,0) = p\mathrm{e}^{-5u/2}\left[-2\varepsilon((4\varepsilon^2-23)\mathrm{e}^{2u} - 4\varepsilon^2 - 1)\cos(\varepsilon u) + ((44\varepsilon^2+35)\mathrm{e}^{2u} - 28\varepsilon^2 - 7)\sin(\varepsilon u)\right], \tag{B.6}$$

$$u^1_y(u,\pi) = \frac{(\kappa_1+1)cp\mathrm{e}^{-7u/2}}{4\mu_1\cosh(\pi\varepsilon)}\left[24\varepsilon(\mathrm{e}^{4u} - \mathrm{e}^{2u})\sin(\varepsilon u) - ((4\varepsilon^2-35)\mathrm{e}^{4u} - (8\varepsilon^2+14)\mathrm{e}^{2u} + 4\varepsilon^2 + 1)\cos(\varepsilon u)\right], \tag{B.7}$$

$$\begin{aligned}u^1_y(0,v) = \frac{cp}{4\mu_1\cosh(\pi\varepsilon)}&24\varepsilon[\cos(v/2) - \cos(3v/2)][(\kappa_1-1)\cosh((\pi-v)\varepsilon) - (\kappa_1+1)\sinh((\pi-v)\varepsilon)]\\ &+[(4\varepsilon^2-35)\sin(v/2) + (8\varepsilon^2+14)\sin(3v/2) - (4\varepsilon^2+1)\sin(7v/2)]\\ &\times[(\kappa_1-1)\sinh((\pi-v)\varepsilon) - (\kappa_1+1)\cosh((\pi-v)\varepsilon)],\end{aligned} \tag{B.8}$$

$$\begin{aligned}u^1_y(u,0) = \frac{(\kappa_1\kappa_2-1)cp\mathrm{e}^{-7u/2}}{2[\mu_2(\kappa_1+1)+\mu_1(\kappa_2+1)]}&\left[24\varepsilon(\mathrm{e}^{4u} - \mathrm{e}^{2u})\cos(\varepsilon u)\right.\\ &\left.+((4\varepsilon^2-35)\mathrm{e}^{4u} - (8\varepsilon^2+14)\mathrm{e}^{2u} + 4\varepsilon^2 + 1)\sin(\varepsilon u)\right].\end{aligned} \tag{B.9}$$

Expressions for stresses and displacements along $y = 0^-$ (which lies in Material 2 and covers $v = -\pi$ for $x \leqslant -c$; $u = 0$ and $-\pi < v < 0$ for $-c < x < c$; and $v = 0$ for $x \geqslant c$) can be obtained based on expressions given above. Specifically, $u^2_y(0,v)$ can be obtained by replacing μ_1, κ_1, $\cosh((\pi-v)\varepsilon)$, and $\sinh((\pi-v)\varepsilon)$ in $u^1_y(0,v)$ with μ_2, κ_2, $\cosh((\pi+v)\varepsilon)$, and $-\sinh((\pi+v)\varepsilon)$, respectively. Also, stresses $\sigma^2_{yy}(0,v)$ and $\sigma^2_{xy}(0,v)$ can be obtained from $\sigma^1_{yy}(0,v)$ and $\sigma^1_{xy}(0,v)$ by replacing $\cosh((\pi-v)\varepsilon)$ and $\sinh((\pi-v)\varepsilon)$ with $\cosh((\pi+v)\varepsilon)$ and $-\sinh((\pi+v)\varepsilon)$, respectively. In particular, the normal displacement u_y along the lower cohesive surface $-c < x < c$ and $y = 0^-$ (i.e., $u = 0$ and $-\pi < v < 0$) is given by

$$\begin{aligned}u^2_y(0,v) = \frac{cp}{4\mu_2\cosh(\pi\varepsilon)}&24\varepsilon[\cos(v/2) - \cos(3v/2)][(\kappa_2-1)\cosh((\pi+v)\varepsilon) + (\kappa_2+1)\sinh((\pi+v)\varepsilon)]\\ &-[(4\varepsilon^2-35)\sin(v/2) + (8\varepsilon^2+14)\sin(3v/2) - (4\varepsilon^2+1)\sin(7v/2)]\\ &\times[(\kappa_2-1)\sinh((\pi+v)\varepsilon) + (\kappa_2+1)\cosh((\pi+v)\varepsilon)].\end{aligned} \tag{B.10}$$

Appendix C. Solutions for anti-plane shear or Mode III

For anti-plane shear or Mode III deformation, $u_x = u_y = 0$ and $u_z = u_z(x,y)$ in the Cartesian coordinate system. The non-trivial displacement and stresses can be written as

$$u^j_z = \mathrm{Im}(X_j(\zeta))/\mu_j, \quad \sigma^j_{zx} = \mathrm{Im}(X'_j(\zeta)), \quad \sigma^j_{zy} = \mathrm{Re}(X'_j(\zeta)), \tag{C.1}$$

where superscript or subscript j refers to material number. The Westergaard function for Mode III deformation is chosen as

$$X'_j(\zeta) = Z_j(\zeta) = \Upsilon_j(\omega) = (\lambda^2-1)(b_j + \mathrm{i}a_j)\mu_j\mathrm{e}^{\lambda\omega}. \tag{C.2}$$

Using Eq. (7) and integrating Eq. (C.2) with respect to ζ yields

$$X_j(\zeta) = \int Z_j(\zeta)\,\mathrm{d}\zeta = \frac{c}{2}(b_j + \mathrm{i}a_j)\mu_j[(\lambda-1)\mathrm{e}^{(\lambda+1)\omega} - (\lambda+1)\mathrm{e}^{(\lambda-1)\omega}]. \tag{C.3}$$

The traction-free boundary conditions at the crack surfaces and the continuity of traction and displacement at the bonded interface ($v = 0$) are

$$\sigma^1_{zy}(u,\pi) = \sigma^2_{zy}(u,-\pi) = 0, \quad \sigma^1_{zy}(u,0) = \sigma^2_{zy}(u,0), \quad u^1_z(u,0) = u^2_z(u,0). \tag{C.4}$$

Substituting Eqs. (C.1)–(C.3) into Eq. (C.4) and solving the equations yields the following eigenvalues

$$\lambda = \frac{n}{2} \quad (n \text{ is an integer}). \tag{C.5}$$

It has been argued that the dominant stresses in the eigenfunction expansion corresponds to $\lambda = -1/2$ (Zhang and Deng, 2005a). Let $\lambda = -1/2$, we can obtain the following stress and displacement fields

$$\sigma^1_{zx}(u,v) = \sigma^2_{zx}(u,v) = -\tau_{\max}\mathrm{e}^{-u/2}\sin(v/2), \tag{C.6}$$

$$\sigma^1_{zy}(u,v) = \sigma^2_{zy}(u,v) = \tau_{\max}\mathrm{e}^{-u/2}\cos(v/2), \tag{C.7}$$

$$u^1_z(u,v) = \frac{\mu_2\delta_{\mathrm{tip}}}{4(\mu_1+\mu_2)}\left[3\mathrm{e}^{u/2}\sin(v/2) - \mathrm{e}^{-3u/2}\sin(3v/2)\right], \tag{C.8}$$

$$u^2_z(u,v) = \frac{\mu_1\delta_{\mathrm{tip}}}{4(\mu_1+\mu_2)}\left[3\mathrm{e}^{u/2}\sin(v/2) - \mathrm{e}^{-3u/2}\sin(3v/2)\right], \tag{C.9}$$

with

$$\tau_{\max} = \frac{3}{4}p, \quad \delta_{\mathrm{tip}} = \frac{(\mu_1+\mu_2)p}{\mu_1\mu_2}c. \tag{C.10}$$

Eqs. (C.6)–(C.9) reveal that the stress field has identical expressions for Materials 1 and 2 (but for different physical domains), and the only difference between the upper and lower domains is in the displacement field.

In the cohesive zone (i.e., $u = 0$), we use $\sigma_{zy}(v)$ to replace $\sigma^1_{zy}(0,v) = \sigma^2_{zy}(0,v)$ in Eq. (7) and compute the displacement jump across the cohesive zone as

$$\delta_z(v) = u^1_z(0,v) - u^2_z(0,-v) \quad (0 \leqslant v \leqslant \pi). \tag{C.11}$$

Thus, if the dominant term is assumed to represent the field in the cohesive zone, the form of the traction–separation relationship will then be

$$\sigma_{zy}(v) = \tau_{\max}[1 - (\delta_z(v)/\delta_{\mathrm{tip}})^{2/3}]^{1/2} \quad (0 \leqslant \delta_z(v) \leqslant \delta_{\mathrm{tip}}). \tag{C.12}$$

References

Aravas, N., Sharma, S.M., 1991. An elastoplastic analysis of the interface crack with contact zones. Journal of the Mechanics and Physics of Solids 39, 311–344.

Atkinson, C., 1977. On stress singularities and interfaces in linear elastic fracture mechanics. International Journal of Fracture 13, 807–820.

Blackman, B.R.K., Hadavinia, H., Kinloch, A.J., Williams, J.G., 2003. The use of a cohesive zone model to study the fracture of fibre composites and adhesively-bonded joints. International Journal of Fracture 119, 25–46.

Comninou, M., 1977. The interface crack. ASME Journal of Applied Mechanics 44, 631–636.

Comninou, M., 1990. An overview of interface cracks. Engineering Fracture Mechanics 37, 197–208.

Deng, X., 1992. Complete complex series expansions of near-tip fields for steadily growing interface cracks in dissimilar isotropic materials. Engineering Fracture Mechanics 42, 237–242.

Deng, X., 1993. General crack-tip fields for stationary and steadily growing interface cracks in anisotropic bimaterials. ASME Journal of Applied Mechanics 60, 183–188.

Deng, X., 1995. Mechanics of debonding and delamination in composites: asymptotic studies. Composites Engineering 5, 1299–1315.

Dundurs, J., 1969. Edge-bonded dissimilar orthogonal elastic wedges under normal and shear loading. ASME Journal of Applied Mechanics 36, 650–652.

England, A.H., 1965. A crack between dissimilar media. ASME Journal of Applied Mechanics 32, 400–402.

Erdogan, F., 1965. Stress distribution in bonded dissimilar materials with cracks. ASME Journal of Applied Mechanics 32, 403–410.

Feraren, P., Jensen, H.M., 2004. Cohesive zone modelling of interface fracture near flaws in adhesive joints. Engineering Fracture Mechanics 71, 2125–2142.

Keer, L.M., Guo, Q., 1990. Stress analysis of symmetrically loaded bonded layers. International Journal of Fracture 43, 69–81.

Lin, K.Y., Mar, J.W., 1976. Finite element analysis of stress intensity factors for cracks at a bi-material interface. International Journal of Fracture 12, 521–531.

Madhusudhana, K.S., Narasimhan, R., 2002. Experimental and numerical investigations of mixed mode crack growth resistance of a ductile adhesive joint. Engineering Fracture Mechanics 69, 865–883.

Maplesoft, 2004. Available from: <http://www.maplesoft.com>.

Mohammed, I., Liechti, K.M., 2000. Cohesive zone modeling of crack nucleation at bimaterial corners. Journal of the Mechanics and Physics of Solids 48, 735–764.

Rice, J.R., 1988. Elastic fracture mechanics concepts for interfacial cracks. ASME Journal of Applied Mechanics 55, 98–103.

Suo, Z., Hutchinson, J.W., 1990. Interface crack between two elastic layers. International Journal of Fracture 43, 1–18.

Symington, M.F., 1987. Eigenvalues for interface cracks in linear elasticity. ASME Journal of Applied Mechanics 54, 973–974.

Timoshenko, S., Goodier, J.N., 1951. Theory of Elasticity, second ed. McGraw-Hill, New York.

Ting, T.C.T., 1986. Explicit solutions and invariance of the singularities at an interface crack in anisotropic composites. International Journal of Solids and Structures 9, 965–983.

Ting, T.C.T., 1996. Anisotropic Elasticity—Theory and Applications. Oxford University Press, Oxford.

Tvergaard, V., 2004. Predictions of mixed mode interface crack growth using a cohesive zone model for ductile fracture. Journal of the Mechanics and Physics of Solids 52, 925–940.

Unger, D.J., 1995. Analytical Fracture Mechanics. Academic Press, San Diego.

Williams, M.L., 1959. The stresses around a fault or cracks in dissimilar media. Bulletin of the Seismological Society of America 49, 199–204.

Zhang, W., Deng, X., 2005a. Formulation of a cohesive zone model for a Mode III crack. Engineering Fracture Mechanics 72, 1818–1829.

Zhang, W., Deng, X., 2005b. Mixed-mode I/II fields around a crack with a cohesive zone ahead of the crack tip (submitted for publication).